

Utilizing Advanced Air Mobility Rotorcraft Tools for Wildfire Applications

Jeremy Aires

Computer Engineer
NASA Ames Research Center
Moffett Field, CA, USA

Shannah Withrow-Maser

Aerospace Engineer
NASA Ames Research Center
Moffett Field, CA, USA

Nicholas Peters

Aerospace Engineer
NASA Ames Research Center
Moffett Field, CA, USA

ABSTRACT

Over the past decade, due in large part to heavy investment in the field of Advanced Air Mobility (AAM), significant progress in rotorcraft-focused modeling tools has been made. Such progress has notably increased AAM rotorcraft modeling capabilities in the topics of conceptual design, preliminary design, and more recently flight dynamics. Yet, due to recent and persistent increases in extreme weather events, an emerging interest has been raised in utilizing such modeling capabilities for aiding in emergency relief efforts and other public good missions. This paper uses wildfire fighting as a representative public good mission and demonstrates the relevance of the NASA Revolutionary Vertical Lift Technology (RVLT) rotorcraft toolchain to such missions. An emphasis is placed on flight dynamics modeling and control because of the hazards and challenges associated with the atmospheric environment of wildfires. In this work, the NASA FlightCODE tool was used to analyze both a UH-60 and the NASA six-passenger quadrotor reference model hovering in an experimentally informed wildfire turbulent environment. Preliminary results of this study estimate actuator usage exceedances and disturbance rejection capabilities of the vehicles' translational rate command systems. Leveraging the RVLT toolchain, refinement and expansion of this work could lead to handling qualities envelope estimation and design optimization for wildfire turbulent environments. This would provide pilots with additional information to make real-time decisions in high-risk scenarios and begins preparations for simulating these dangerous environments for pilot training and experimentation.

INTRODUCTION

Software tools for rotorcraft vehicle design have undergone significant development with a primary focus on supporting the Advanced Air Mobility (AAM) field in the last decade. As a result, there now exists a notable expansion in analysis capability in the conceptual design stage of a vehicle's life cycle. This has enabled the inclusion of key parameters in the early stages of rotorcraft design such as vehicle aeroelastic characteristics, aeroacoustics signatures, and rotor optimization in edge-case scenarios. Flight dynamics and controls is another area which has experienced an expansion in analysis capabilities including handling qualities predictions, disturbance rejection effectiveness, and atmospheric turbulence influence on actuator utilization. With the buildup of these flight dynamics prediction abilities, there exists a significant interest in leveraging existing tools for the analysis of not only AAM vehicle design, but for public good missions as well (Ref. 1). In support of furthering the application of modern design tools to public good missions, this study was performed focusing on two rotorcraft in a simulated wildfire emergency response scenario. The feasibility of including vehicle flight

dynamics in turbulent environments informed by wildfire conditions into the early stages of vehicle design was evaluated. The objective of this paper is not only to explore an approach for analyzing vehicles operating in the wildfire environment but to help further community research in general for public good missions. Such emergency relief efforts not only benefit the public but also help build confidence in new vehicle capabilities and platforms that can be applied to the public sector.

BACKGROUND

Motivation

Helicopters are critical to firefighting efforts, and a logical vehicle selection for low-altitude, variable terrain, high risk missions. As part of the "This Day in History" series, the National Wildfire Coordinating Group (NWCG) emphasized the importance of helicopters in wildfire fighting:

The helicopter has proven to be a valuable tool in wildland fire operations and support for many years, transporting firefighters, moving cargo and equipment, dropping water and retardant, flying reconnaissance and observation missions, aerial ignition work, long lining, and simply providing eyes-in-the-sky fire information to the incident commander or burn boss. There

Presented at the Vertical Flight Society's 80th Annual Forum & Technology Display, May 7-9, 2024, Montréal, Québec, Canada. This is a work of the U.S. Government and is not subject to copyright protection in the United States.

are few fires where this aviation resource is not utilized in some capacity (Ref. 2).

Helicopters have been used in the efforts to battle wildfires since 1946 (Ref. 2). Despite the longevity, only recently has the interest to really understand how rotorcraft operate in a wildfire environment been renewed. This renewed interest has likely been influenced by increased wildfire activity in recent years as well as the expanded coverage of such events via social media. California, Texas, and Hawaii, as well as many other locations worldwide, have been in headlines recently for massive evacuations and losses due to wildfires. A more in-depth review on these events as well as technology gaps for rotorcraft as a whole in the wildfire environment were discussed in work presented earlier this year (Ref. 3). Wildfire modeling is extremely complex because of their dynamic. Recent advancements in reducing computational time and increasing the flexibility of tools, enables access to a larger range of higher fidelity datasets that could potentially inform future aircraft-based wildfire fighting efforts.

In 2015, the CDC released a summary of aviation-related wildfire firefighter fatalities from 2000-2013 (Ref. 4). Within this time frame, 78 aviation-related fatalities occurred. Of the 42 vehicles involved, 23 (55%) were fixed wing aircraft and 19 (45%) were helicopters. For those where the pilots in command were victims, each pilot had a mean total of 10,725 flight hours (flight hours were based solely on flight hours for the U.S. Forest Service). The four reported leading causes of fatality all have flight dynamics or handling qualities implications:

The leading causes of fatal aircraft crashes were engine, structure, or component failure (24%); pilot loss of control (24%); failure to maintain clearance from terrain, water, or objects (20%); and hazardous weather (15%) (Ref. 4).

A key factor driving up the complexity associated with operating in the wildfire environment is the higher severity of turbulence present in the atmosphere. Previous studies have demonstrated that as the atmospheric flow interacts with the wildfire, several distinct large-scale and high-energy gusts are formed (Ref. 5). Further studies have additionally demonstrated how wildfires not only generate their own distinct flow fields, but also amplify the turbulence that already exists in the flow field (Ref. 6). Due to buoyancy effects, gusts generated by wildfires do not simply exist at low altitudes, but remain coherent as they rise in altitude. Multiple sources have measured large gust (30 ft/s to 164 ft/s velocity perturbations) at altitudes as high as 16 knots (Refs. 7 and 8). Given the high levels of turbulence present in the wildfire environment, it is clear that any wildfire-based rotorcraft analysis must include a sufficiently accurate turbulence model.

Furthermore, it must be emphasized that historically the successful expansion of rotorcraft operational envelopes has typically hinged on the accessibility of computationally efficient and sufficiently accurate turbulence modeling approaches, Refs. 9-15, discussed as follows. These approaches must be capable of providing relevant predictions of the targeted operational environment at a minimal computational cost such that both early-stage conceptual designs can be analyzed, and real-time flight simulations can be conducted. This challenge of deriving meaningful low-order turbulence models has long been an area of focus in the rotorcraft community (Refs. 9 and 10). Limited examples of such mission profile expansions within which turbulence modeling has played a crucial role include offshore oil platform transports (Ref. 11), shipboard operations (Ref. 12), and more recently the operation of rotorcraft in urban environments (Refs. 13, 14, and 15). For each example, the fidelity of turbulence models has played a critical role in pilot training and remains an active field of research to this day (Ref. 13).

If turbulence and vehicle models are sufficiently representative of real-world wildfire conditions and aircraft, it is proposed that RFLT tools could be repurposed to inform vehicle design and/or training methods. In order to apply the toolchain to these events, the following technology gaps were identified: insufficiently accurate modeling of wildfire-driven turbulence and vehicle interaction dynamics that can be simplified to run in a real-time simulation, lack of data on pilot workload and its impact on handling qualities, insufficient tailored mission task elements and visual environment scales, and handling qualities of the aircraft after component failure. This work will explore atmospheric modeling, vehicle modeling, and handling qualities of vehicles operating in a wildfire environment with other aforementioned research efforts left to future work.

Existing Software Tools

NASA's RFLT Project's toolchain is comprised of rotorcraft-focused design and analysis software that will be referred to as the "RFLT toolchain" for the remainder of this paper. One goal of the tool chain is, "to provide robust computational methods that facilitate design space exploration with varied problem definitions and with the ability to concurrently consider several different potential solutions" (Ref. 16). Ref. 16 describes additional tools available as part of the toolchain; however, this study was focused on the impact of handling qualities in the design process. The applicable components of the toolchain were Comprehensive Analytical Model for Rotorcraft Aerodynamics and Dynamics (CAMRAD II) for rotor design, NASA Design and Analysis of Rotorcraft (NDARC) for vehicle sizing, and FlightCODE (formerly known as SIMPLI-FLYD) (Refs. 17, 18, and 19). The use of FlightCODE is key to this study as it produces reduced-order, linearized models appropriate for use in control system design. It should be noted that FlightCODE is still

under development and not publicly available at the time of writing. For this study existing NDARC vehicle models were repurposed; however, the same approach could be utilized for a novel vehicle concept. In that case, NDARC and CAMRADII would be used iteratively until a design closed for the given mission parameters. From there, using the NDARC design as an input, the vehicle models can be furthered analyzed in FlightCODE. While not formally part of the tool chain, an additional step in the analysis could be to feed the bare airframe from FlightCODE and a controller into CONDUIT to automate the gain tuning process based on handling qualities metrics of interest.

Applicable Lessons from Previous Handling Qualities Testing in a Motion-Based Simulator

Like wildfires, AAM missions are also high pilot workload scenarios. A key finding from a 2021 Urban Air Mobility (UAM)-focused Vertical Motion Simulator (VMS) study (Ref. 13, 15) that is relevant to this work is the impact of pilot workload on handling qualities ratings. In many scenarios pilots were able to achieve the maneuver criteria in “desired” parameters but felt that handling qualities ratings in the “adequate” range were more appropriate because of the pilot workload required (or that adequate criteria were achievable, but only with an unacceptable workload). High workload can be inherent to aerial firefighting missions due to a number of factors including tracking the fire, communication with support crews, awareness of other vehicles in the area, flying low in challenging terrain, degraded visuals from smoke, changing weather conditions, etc. Thus, it would be logical to focus future efforts on how best to relieve workload from the pilot through implementation of features like higher control mode augmentations, such as translational rate command (TRC) which has been previously shown to improve both handling and ride qualities for a hover mission task element (MTE) with turbulence (Ref. 13).

It is well understood that turbulence affects performance, which in turn impacts handling qualities. While there was some degradation in handling qualities consistently reported with turbulence in the same 2021 UAM VMS simulation (Ref. 13, 15), a follow-up UAM VMS simulation in 2023 (Ref. 14) identified that accurately modeling turbulence levels was a key aspect of the simulation. A crucial difference between the 2021 and 2023 tests was that no limits were imposed in the 2021 version of the UAM VMS test, while actuator and power limits were modeled in the later VMS entry. When turbulence was added during the 2023 VMS test, actuator and/or power limits were frequently encountered which resulted in more obviously degraded handling qualities. Extrapolating from this finding, it can be concluded that, as wildfires are gust and turbulent rich environments, the accurate modeling of the atmospheric environment is critical as well as modeling mechanical limits of the vehicle. These findings influenced the assumptions of this wildfire study.

PRELIMINARY WILDFIRE STUDY

As mentioned earlier in the Background section, the ability to hover gives firefighting rotorcraft a distinct advantage for performing unique tasks such as reconnaissance and precise retardant drops. Important considerations for these types of missions are environmental disturbances like turbulence and wind. Thus, this preliminary study aims to assess the control authority and actuator usage of firefighting vehicles as they hover in a turbulent environment. A representative wildfire turbulence model was developed and compared against a Dryden model for light turbulence. This model was used in previous work and serves to baseline the results. Furthermore, by showing a range of potential turbulences, an estimated range for expected control authority and actuator usage can be encapsulated. This will be discussed further in the Results and Conclusions sections.

Two vehicles were chosen for this study: a UH-60 Black Hawk and a conceptual AAM quadrotor designed by NASA RVLТ. The UH-60 was selected because a derivative of its design, the S-70 Firehawk, is commonly used for firefighting missions. The conceptual AAM quadrotor was chosen to assess the feasibility of adapting eVTOL technology from the AAM market to public good missions.

As discussed in the previous section, a TRC augmentation provides a level of autonomy to the vehicle which has the potential to reduce pilot workload and improve handling qualities. Implementing this response type is also beneficial in terms of showcasing the disturbance rejection capabilities of the vehicles. This was accomplished by running 100 five-minute simulations for both vehicles in the two levels of turbulence. Additionally, each of these tests was run once more (8 in total) to understand the effects of adding a constant, 22.96 ft/sec (13.6 knot) headwind to the simulation. This value represents a mean wind from a wildfire as measured in experiments by Seto, et al. (Ref. 20).

Turbulence Modeling Approaches

In this study, two turbulence modeling approaches were selected for generating disturbance inputs. Following previous work, the first turbulence model used in this study is that of the Dryden turbulence model with low speed, low altitude corrections applied (Ref. 15). The corrections applied to the Dryden model in this study are consistent with previous implementations of the model. Namely, these corrections include selecting settings for a mean wind speed of 15 kts at 20 ft altitude as specified by the low altitude Dryden specification (Ref. 22). Given that this implementation of the Dryden model has been previously implemented in VMS simulations, and thus subjected to pilot feedback, this initial turbulence model is used to provide the readers with a comparable baseline understanding of how both vehicles should respond in a

light level of turbulence. It must be further highlighted that in this study, only translational velocity perturbations generated by the Dryden model were implemented. As will be discussed, only translational velocity perturbation information was identified to derive the wildfire-based model. To achieve a one-to-one comparison between the Dryden and wildfire-based turbulence models, angular rate perturbations were neglected from the Dryden model.

To gain a preliminary understanding as to how each vehicle will respond in a representative wildfire-driven turbulent flow field, a second turbulence model is used in this study. To generate the second model, a sum of sines approach was selected (Refs. 23 and 24). In this approach, a desired PSD distribution to be emulated is first prescribed using experimental measurements as recorded by Seto et. al. (Ref. 20). In their work, experimental measurements were reported for velocity perturbations as generated through four distinct experimental efforts. Measurements, as reported for experiment two, are used to generate the wildfire turbulence model as this experiment recorded the largest mean wind speed and longitudinal/lateral velocity perturbations. This served as a worst-case scenario for testing the augmented control system, as will be discussed later. For this experiment, velocity perturbations were measured in 2010 for a grass fire with a burn size of five acres. Measurements were recorded at an altitude of 100 ft over a time interval of 30 minutes. While experimental measurements exist before the fire front, during the fire front, and after the fire front, only measurements for during the fire front are used such that a worst-case scenario could be represented.

After selecting the desired PSD, the area under the curve is computed to obtain the variance of the signal (σ_{RMS}^2). In the below equation f is the PSD and ω is the frequency,

$$\sigma_{RMS}^2 = \int_0^{\infty} f(\omega) d\omega. \quad (1)$$

This expression is approximated by the discrete form:

$$\sigma_{RMS}^2 = \sum_{n=1}^{\infty} f(\omega_n) \Delta\omega. \quad (2)$$

It is also known that the root mean square (RMS) of any single sine wave can be computed from the sine wave's amplitude, A , using

$$\sigma_{RMS} = \sqrt{\frac{A^2}{2}}. \quad (3)$$

Assuming orthogonally between the sine waves, the RMS of a series of waves can then be computed using the equation below where A_n is the amplitude of each sine wave,

$$\sigma_{RMS} = \sqrt{\frac{\sum_{n=1}^m A_n^2}{2}}. \quad (4)$$

Thus, by setting equation 2 equal to equation 4, the below relationship can be used to extract the corresponding cosine amplitude for a given PSD distribution,

$$A_n = \sqrt{2f(\omega_n)\Delta\omega_n}. \quad (5)$$

Turbulence predictions can then be made through a summation of each sine wave. In the below equation, u is the velocity perturbation to be modeled, m is the total number of sine waves, t is time, and ϕ_n is a random phase shift applied to each sine wave,

$$u = \sum_{n=1}^m A_n \sin(2\pi\omega_n t + \phi_n). \quad (6)$$

It should be noted that the sum of sines approach ultimately assumes a sufficient expansion of sine functions are used to model the underlying PSD. While the exact number of required sine functions is highly dependent on the desired PSD curve to replicate, in this study given the low computational cost of the model all wildfire turbulence-based simulations were completed using 300,000 sine waves. As will be discussed further in this section the selected number of sine waves were shown to provide a sufficient replication of the prescribed PSD.

While the selected experimental measurements were invaluable in deriving a simplified low-order turbulence model, one limitation of the experimental data was the frequency range reported. It should be noted that the original experimental data set was not derived with the intention of application to rotorcraft flight dynamics. As such the limited sampling rate ultimately places the Nyquist frequency within the range of desired frequencies for flight dynamics (i.e. 0.1 to 20 Hz). Fortunately, further observation of the presented data demonstrates that the turbulence at the Nyquist frequency lies within the -5/3 turbulent energy decay regime. As such, it was assumed that the experimentally measured flow field would stay within the -5/3 energy decay up to a frequency of 20 Hz. A visualization of both the original experimental measurements and the sum of sines-based turbulence model are presented in Fig. 1.

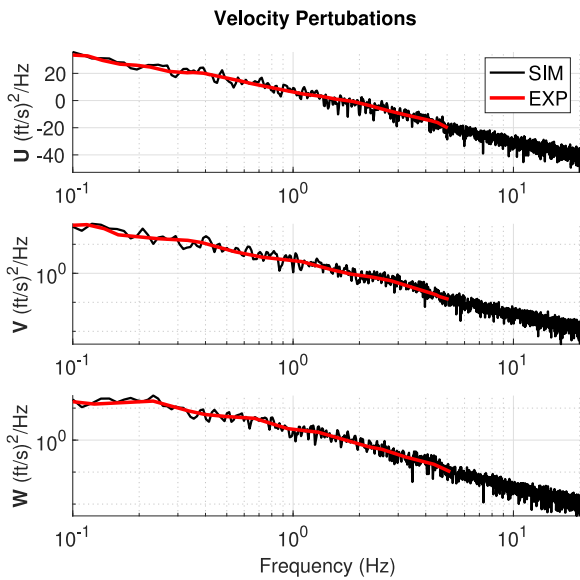


Fig. 1. A comparison of PSDs between the original experimental data (EXP) and the sum of sines model (SIM).

To gain an appreciation for the significant magnitude difference between the wildfire and light Dryden turbulence model, PSDs of both models are provided in Fig. 2. Further plotted are the moderate and severe turbulence levels as reported in Ref. 37. Results clearly show the significant increase in turbulence between the light Dryden model, which has roughly a 1.5 ft/s RMS in the heave axis, and the wildfire turbulence model, which has roughly a 10 ft/s RMS in the heave axis. Additionally, Fig. 2 further shows the close comparison between the wildfire model and what has historically been classified as severe levels of turbulence through the Dryden model. The comparison clearly demonstrates the significant levels of turbulence associated with navigating the wildfire

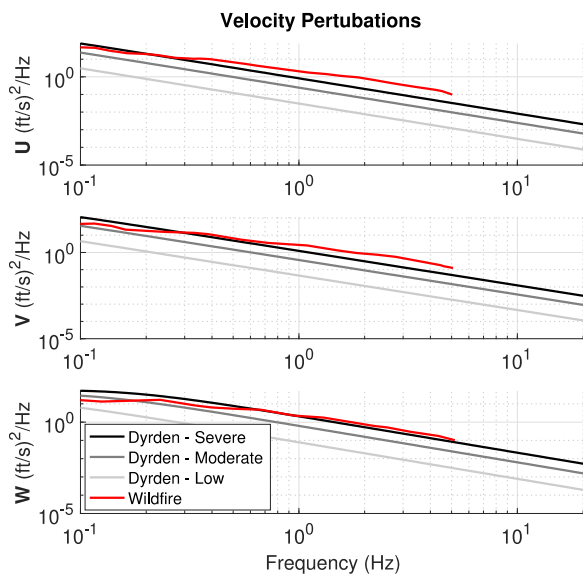


Fig. 2. A comparison of PSDs for wildfire and Dryden model velocity perturbations.

environment, even when neglecting effects such as gusts and limited visibility, effects on which further efforts must be focused to improve the fidelity of the simulated environment.

RVLT Toolchain Vehicle Models

The UH-60 used for this study originated from NDARC and was linearized using FlightCODE to retain first order inflow and flapping dynamics, rigid body states, and Euler angles. This model was ultimately chosen because of its readily available linearization points across forward airspeed. To gain an understanding of the fidelity of the model, frequency response validation comparisons at hover were ran against a 26-state FORECAST model (Ref. 25). Additional dynamics for the FORECAST model included second-order lead/lag and flapping dynamics as well as states for tail rotor inflow, main rotor speed, and main rotor azimuth position. Comparisons for the on-axis pitch and roll responses are shown in Fig. 3. Additional comparisons are available in Appendix A.

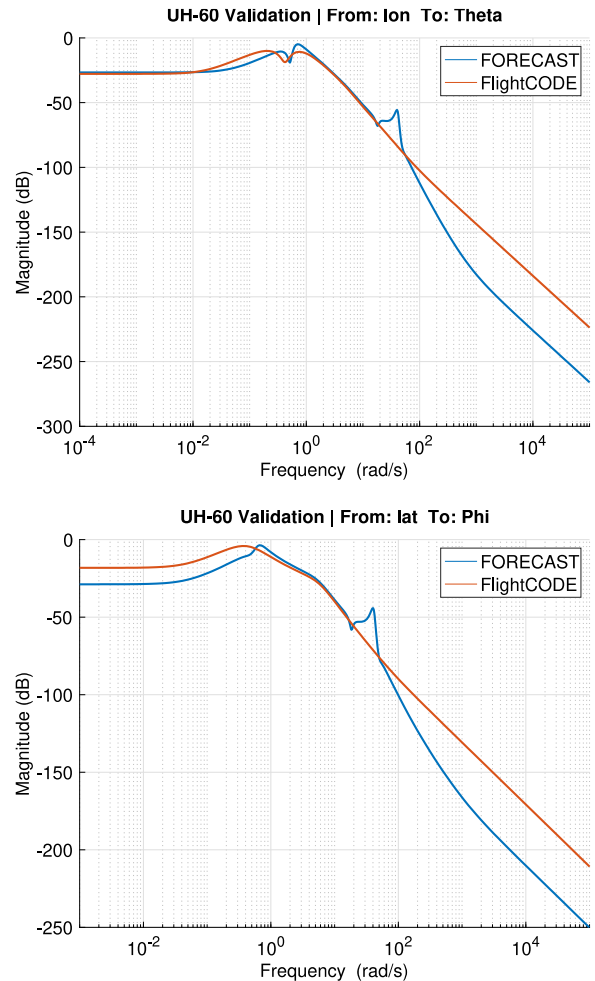


Fig. 3. UH-60 FlightCODE frequency response validation cases against FORECAST for pitch and roll.

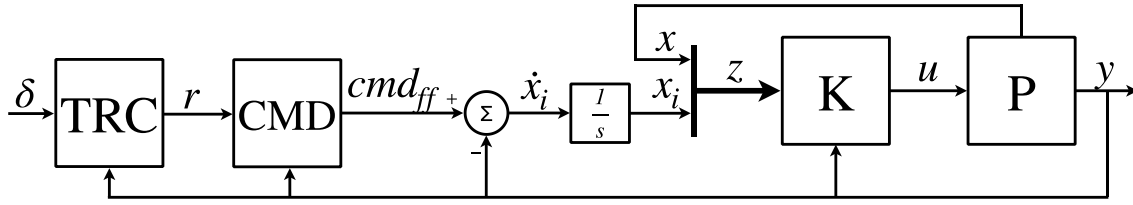


Fig. 4. Simplified block diagram of the flight control system. Here the “P” block represents the nonlinear GPLPV model and actuator dynamics.

The quadrotor was developed in a similar manner to the UH-60 model, with the exception that the predecessor to FlightCODE, SIMPLI-FLYD was utilized. The linearized quadrotor model included first-order flapping dynamics, rotational rates for each of its four rotors, rigid body states, and Euler angles.

Implications for Flight Control, Vehicle Dynamics, and Handling Qualities

Prior to formulating a control law, second-order transfer functions representing additional vehicle dynamics for servo actuators were used to supplement the bare-airframe models. The UH-60 servos were modeled with a natural frequency of 16π rad/sec while the quadrotor used a natural frequency of 42 rad/sec. Both vehicles had a damping ratio of 0.7. Both vehicles were also modeled with saturation limits on the servo positions and rates. Although these limits were not imposed for the purposes of this study, their values were used to normalize actuator usage for each of the vehicles which will be presented later in this work.

With these higher order dynamics incorporated, a linear quadratic integral (LQI) control law was formulated for the FlightCODE UH-60 model to match the architecture used for the quadrotor in previous work and depicted in Fig. 4 (Ref. 14). Linear quadratic controllers are extremely useful because designers can more directly affect change on particular states and inputs of interest by adjusting cost terms for the state and input cost matrices (Q and R, respectively) subject to the cost function,

$$J(u) = \int_0^{\infty} (z^T Q z + u^T R u + 2z^T N u) dt. \quad (7)$$

To simplify the development for this study, the cross-term matrix, N, was set to zero and the input cost matrix, R, was kept at unity.

The chosen baseline response type for the vehicles was ACAH-RCDH-RCHH¹. SAE AS94900 standards were applied to the UH-60 to obtain gain and phase margins of

at least 6 dB and 45°, respectively (Ref. 26). Additionally, disturbance rejection bandwidth (DRB) and peak (DRP) metrics for the on-axis responses (roll, pitch, yaw, and height) per MIL-DTL-32742(AR) were also chosen as requirements (Ref. 27). These were achieved by using a custom optimization routine to tune the controller by manipulating the diagonal terms of the state cost matrix, Q. During an initial hand-tuning exercise it was found that adding cost to the u, v, and w terms of Q seemed to degrade system responses. As such, these terms were kept at zero and eliminated from the optimization routine.

Once the optimization was completed for hover, the new gains were used as an initial condition and the process was repeated for linear models which varied in increments of 20 knots of forward airspeed up to 60 knots. If a set of gains satisfied the stability margin and disturbance rejection requirements for a new airspeed, the optimization routine would record the gains as valid and recycle them once again as an initial condition for the next airspeed. Otherwise, the routine would calculate a new set of gains, record them for the current airspeed, and use them as an initial condition for the next linearized system. This routine was run twice to test the final set of gains across each of the linearized models. The purpose of this was to obtain a single set of weights for the Q matrix and reduce the likelihood for significant variation in the gains, which would eventually be linearly interpolated across forward airspeed. The resulting gains used for the LQI controller are represented by the “K” block in Fig. 4.

One unique feature for the quadrotor was that it had its linear, bare-airframe dynamics stitched together across forward airspeed using a Gaussian process (GP). This concept was adopted from work by Schuet, et al. (Ref. 28) to form a Gaussian process linear parameter varying (GPLPV) model which provides a balance between data fitting and smoothing. Additionally, the GPLPV model also integrated nonlinearities into the system including rigid body, gravitational, and Coriolis terms. The same methodology was also adopted for the UH-60 model to provide a higher level of fidelity for the dynamics at play.

With a nonlinear GPLPV plant and a gain scheduled LQI in place, the inner loop for the flight control system was complete. Loop shaping for this system was provided by a command model on the feedforward path represented by the “CMD” block in Fig. 4. The command model was

¹Attitude Command Attitude Hold (for pitch and roll control), Rate Command Direction Hold (for directional control), and Rate Command Height Hold (for altitude control).

constructed by fitting second-order systems to the four on-axis responses of the inner loop LQI system. These transfer functions were inverted and made causal by multiplying them by another set of second-order filters which allow users to fine tune the system to meet additional handling quality requirements. This is accomplished by manipulating the natural frequency and damping ratio terms. In another effort to simplify the design process for this work, the damping ratios were kept at unity and only the natural frequencies were varied.

The UH-60 model was tuned to achieve Level 1 performance for small and moderate amplitude metrics per ADS-33E-PRF to align with the RVLTL quadrotor. A compilation of these comparisons can be found in Appendix B. The largest difference between the vehicles is that the quadrotor used the same 0.9 rad/sec DRB requirement for both pitch and roll while the UH-60 was only held to the DRB requirements in MIL-DTL-32742(AR) of 0.5 and 0.9 rad/sec for pitch and roll, respectively (Ref. 53). Final DRB values following the optimization method described earlier can be found in Table 1. A similar contrast was also observed in the small-amplitude performance metric for the two vehicles (see Fig. 5).

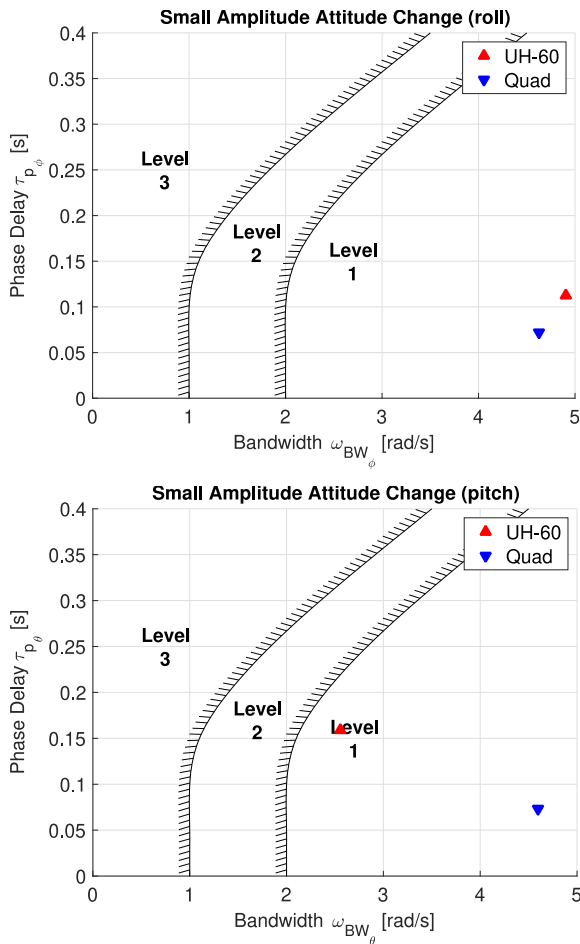


Fig. 5. Small-amplitude roll & pitch performance for the UH-60 and quadrotor.

Table 1. Hover DRB Characteristics [rad/sec]

	ACAH		TRC	
	Pitch	Roll	Surge	Sway
UH-60	0.6276	0.9674	0.3405	0.5428
Quad	0.9031	0.9055	0.3361	0.3354

Lastly, the UH-60 model was augmented with a TRC control mode due to its expected usefulness in firefighting scenarios. For this study, the augmentations for both vehicles consisted of a PI controller with TRC specific modifications to the command model natural frequencies for the longitudinal (surge) and lateral (sway) axes. The TRC and RCHH response types were both tuned to achieve Level 1 performance based on work by Franklin and Stortz (Ref. 29). For this effort, the quadrotor fell just outside the lateral translation boundary (see Fig 6). In terms of DRB, the UH-60 was able to attain the minimums of 0.34 and 0.54 rad/sec for surge and sway, respectively, but the quadrotor was not. The TRC DRB values are summarized in Table 1.

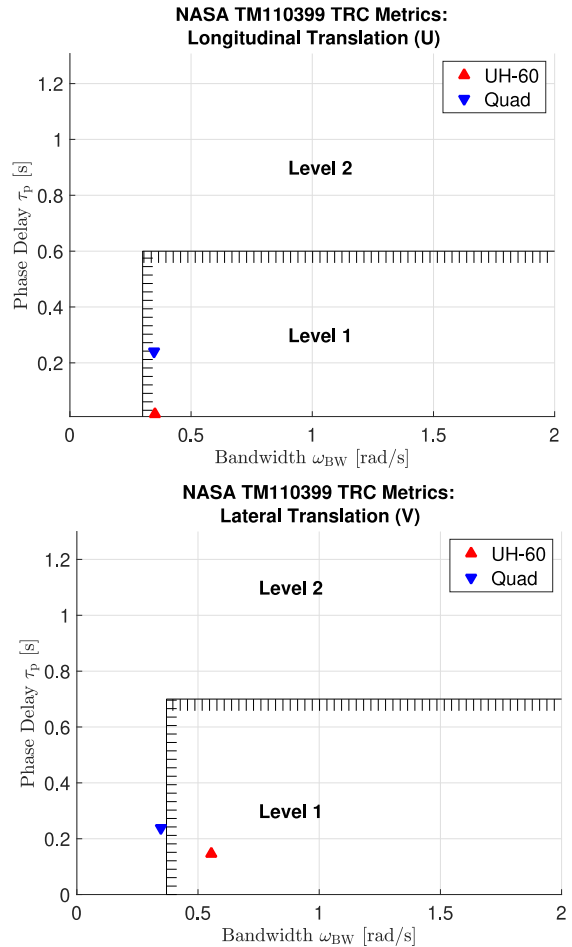


Fig. 6. Translational rate command performance specifications for the UH-60 and quadrotor.

RESULTS & DISCUSSION

With the control systems for the vehicles designed, the 100 five-minute simulations for each of the eight test cases described in the “Preliminary Wildfire Study” section were run. It is worth noting that the turbulence and wind disturbances were ramped in over the first five seconds to prevent unintended spikes in the data. Fig. 7 shows the disturbance rejection capabilities of the TRC augmentation for the two vehicles in terms of positional deviations from the initial hover point (represented by the origin) for the light and wildfire turbulence-only conditions. Principal component analysis (PCA) was also performed to illustrate the statistical spread of the data without constraint to the XY ground plane. The first two principal component directions are represented by black and yellow lines, respectively. Red ellipses represent the spans of the first three standard deviations of the data along the principal component directions. Single standard deviation values

along for the first two principal component directions are listed in the legends for each plot.

For both the wildfire and light turbulence conditions, the quadrotor was able to maintain a tighter hold on the hover location while the UH-60 drifted further, primarily along the longitudinal direction. Mechanisms within the control system are suspected to be the main cause for this behavior. Further analysis showed that a 20 second longitudinal TRC step response had a steady-state error of approximately 4.6% compared to 2.0% for the lateral axis. Attempts to resolve this issue were unsuccessful with lower proportional gains only exacerbating the offset, even without integral action. Manipulations of the command model natural frequency were also fruitless. Inspection of the inner-loop system revealed oscillatory behavior in the ACAH step response for the longitudinal axis. This may be a result of mismatches between the GPLPV stitched plant and the linearly stitched LQI gains. Furthermore, the fits used for the command model were also stitched linearly

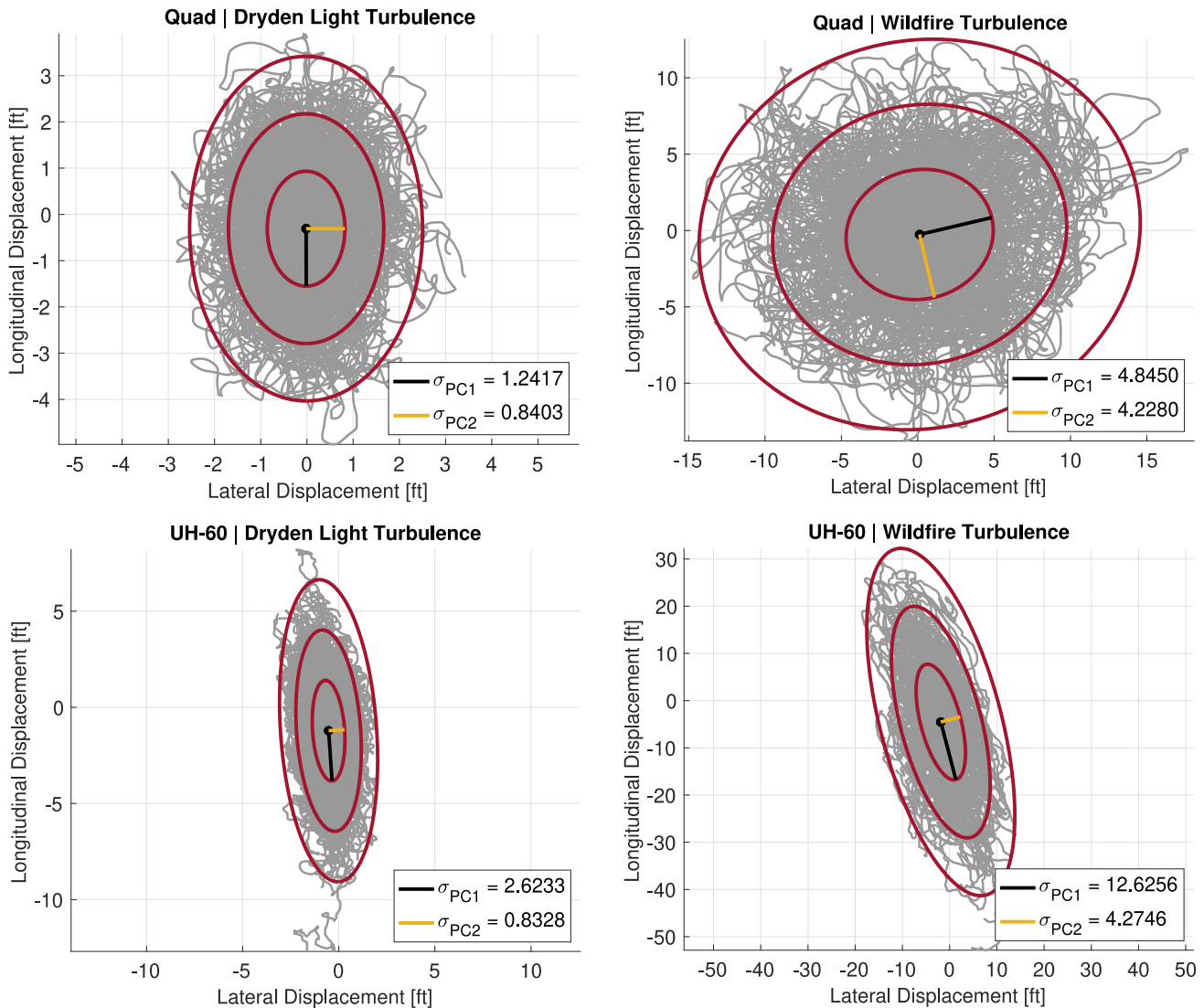


Fig. 7. XY-positional deviation comparisons for turbulence-only cases.

with airspeed and could be another source of error. Finally, as mentioned earlier, there is also an inner-loop ACAH DRB discrepancy for the pitch axis between the quadrotor and UH-60 which could certainly be contributing to the longitudinal elongation (see Table 1).

Another observation from Fig. 7 is that the spread of the UH-60 data appeared rotated, slightly counter-clockwise of the longitudinal axis. The average heading deviation for the UH-60 was slightly negative for all cases, but the magnitude appears to be negligible (see Table D1 in Appendix D). One explanation could be control system configuration differences between the pitch and roll axes as described in the last paragraph or an inherent dynamic coupling in the system. To gain an appreciation for the scale and relativeness of these positional deviations, the ellipses representing three standard deviations of the PCA for each turbulence combination have been overlaid together in Fig. 8.

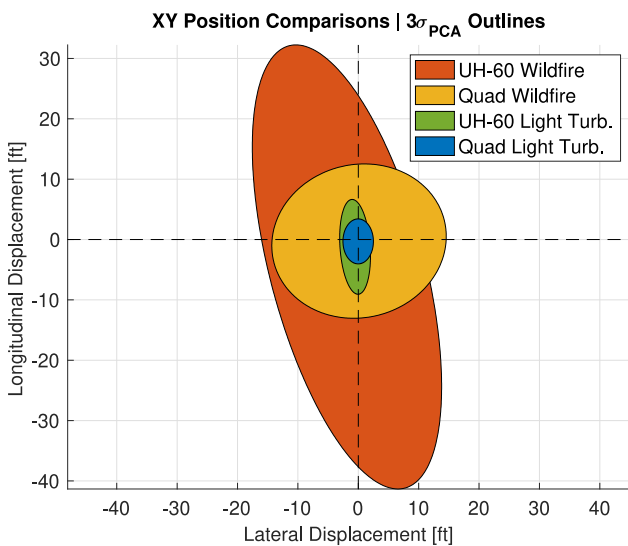


Fig. 8. XY-positional deviation comparisons using PCA.

In addition to the turbulence-only cases, the inclusion of a 22.96 ft/sec headwind was introduced to each of the combinations to assess the additional effort and performance of the vehicles. Results for the XY-positional deviations in wildfire turbulence with wind are presented in Fig. 9 while light turbulence with wind cases can be found in Appendix C.

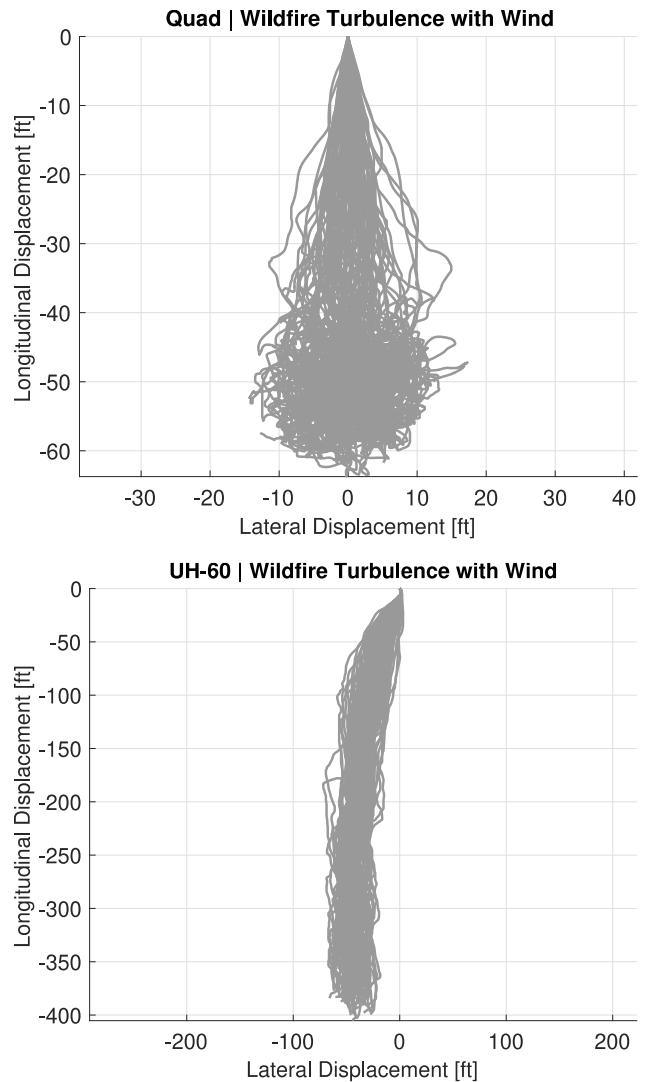


Fig. 9. XY-positional deviations in wildfire turbulence with wind.

Deficiency of the TRC designed for the UH-60 is visible in Fig. 9 where the traces for all 100 cases drift aft as far as 400 feet from the initial position with an average airspeed (a.k.a. TRC surge error) of -1.0334 ft/sec. Again, this is likely a control system deficiency with causes like those described earlier for the turbulence-only results. Conversely, the quadrotor was able to eventually compensate for the additional disturbance and only drifted approximately 50 feet aft of the initial hover point. Additional statistics on deviations for each of the controlled axes can be found in Appendix D.

Actuator usage was collected for the vehicles in the various conditions. Theoretical limits for the actuators were not imposed for these simulations, but they were used for normalizing the data seen in Fig. 10. Additionally, both vehicles were initialized in hover with the assumption that the actuators were at the center position with an equal range of motion. As such, normalization for the usage was performed on the absolute value of the actuator data.

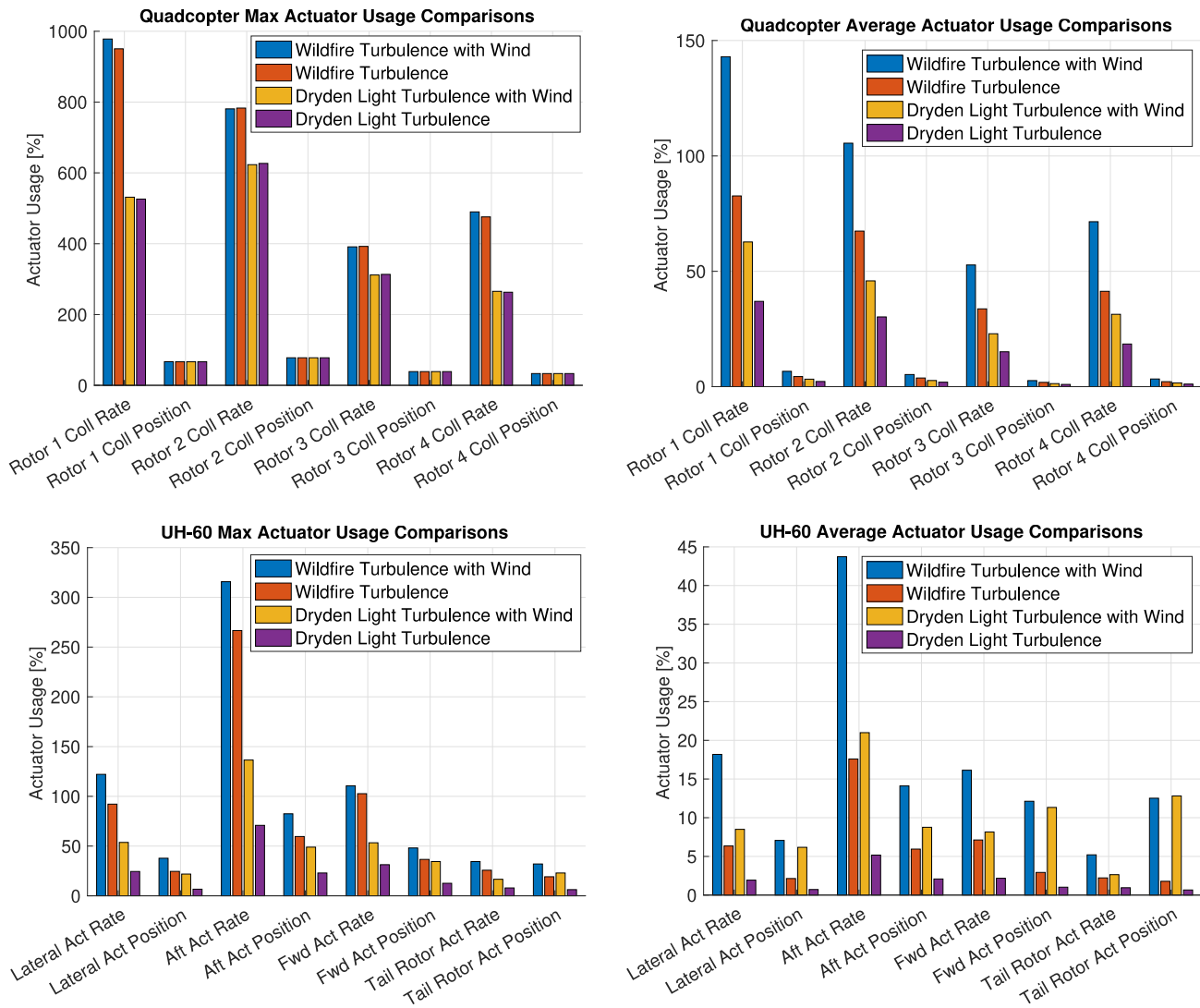


Fig. 10. Maximum (left) and average (right) actuator usage comparisons for the quadrotor (top) and UH-60 (bottom).

The maximum use cases present the single maximum values for each axis across all 100 simulations. For the UH-60, the order of limiting actuators begins with the aft actuator, followed by the lateral and forward actuators with comparable usages, and ending with the tail rotor actuator. Although the UH-60 slightly exceeds tolerances for aft actuator rate usage in the light turbulence case (136.5%), it is plausible that the control system could be redesigned with saturation considerations while maintaining Level 1 handling qualities. However, wildfire conditions demanded over 250% usage of the aft actuator which might not be reducible (while maintaining Level 1 metrics) with control system redesign alone. In terms of average actuator usage, the introduction of the headwind into the system certainly offset positional usage percentages for all actuators, which makes sense given that the constant disturbance keeps the vehicle regularly displaced from its trimmed hover condition.

For the quadrotor, front rotors 1 (right) and 2 (left) were the most restrictive. Nonetheless, while rear rotors 3 (right)

and 4 (left) were the least restrictive, they each still caused the quadrotor to exceed its rate limits by 250% for all test conditions. The addition of wind did not have a significant effect on the maximum rate values for the quadrotor, but they did have a higher average usage compared to their respective, turbulence-only test cases. Average actuator usage for the quadrotor consistently decreased for both positions and rates alongside test cases of decreasing disturbance magnitudes (from wildfire turbulence with wind being the most disruptive to the light Dryden turbulence without wind being the least). This is because the collectively controlled quadrotor is mixed to impart motion on all four rotors regardless of the input from the controller (i.e., effective collective, lateral cyclic, longitudinal cyclic, and pedal commands).

One factor affecting turbulence severity is the vehicle position relative to the wildfire. Since the representative wildfire turbulence chosen for this study was based on measurements during a fire front passage (essentially, within the fire), it was assumed that the expected severity

encountered by a vehicle lies somewhere between the light and wildfire models. Thus, approximate ranges for the vehicles' controller performance and actuator usage can be established. Controller performance was assessed using the max, three standard deviation range of position in any direction. In turbulence-only scenarios, the quadrotor had a displacement range of about 4-15 feet while the UH-60 had a range of approximately 8-38 feet. Note that these PCA ranges are with respect to the mean XY-position values for each dataset, not the initial hover location (origin). To account for this, the Euclidean norm distance between these means and the origin were added to the estimated ranges. This did not significantly change the results for the quadrotor, but it did enlarge the UH-60 range to be 9-43 feet. Asides from a transient phase where the vehicle drifted rearward about 50 feet, the addition of wind did not appear to significantly affect these ranges for the quadrotor. This transient drift is in some respect artificial because of the way the headwind is ramped into the system for an aircraft trimmed at hover. Assuming the required control authority would be available, and based on the steady-state controller performance observed in Fig. 11, it appears that drifts from steady winds would be correctable with pilot compensation. A similar plot for the quadrotor in the light Dryden turbulence scenario can be found in Appendix C.

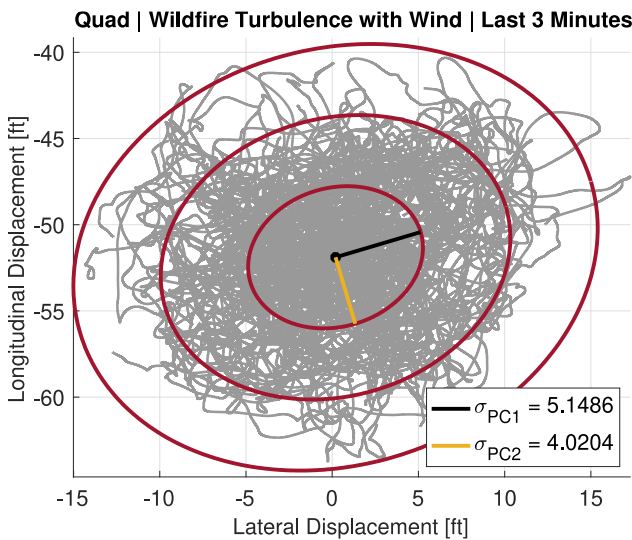


Fig. 11. PCA for the last three minutes of the quadrotor in wildfire turbulence with wind.

Again, the drift experienced by the UH-60 (see Fig. 9) is likely due to a controller deficiency and it is hypothesized that, once corrected, similar results should be obtainable. Approximate actuator exceedances for the UH-60 ranged from 130-320% while the quadrotor ranged from 620-980%. These are based on max usage values for the turbulence with wind cases for the light Dryden (lower limit) and wildfire (upper limit) models.

Overall, the quadrotor had good positional tracking, but the current design is not feasible given the large actuator

exceedances. While the control system should be redesigned with consideration given to the actuator limits, the higher end of the actuator exceedance estimate is almost an order-of-magnitude greater than the design point. This may indicate that the vehicle itself cannot provide enough control authority and needs to be resized.

NEXT STEPS

It is recommended that these studies be expanded by including feedback from certified wildfire pilots and that any data generated from these efforts be formatted in a way that is easily accessible by the public, so that a wider range of data is available. An appropriate next step for expanding such a data set would be maturing the controller design and appropriate handling qualities metric criteria.

The controller design should be revisited to resolve the inner-loop ACAH oscillations and tighten the outer-loop TRC performance. Subsequently, consideration and comparison of additional higher level augmentation control modes (e.g., position hold) could help determine best practices for reducing pilot workload. Ride quality must also have some consideration. It is possible the controller could cause the vehicle to be too reactive to the environment to the point that the pilot experienced extreme accelerations or vibrations.

To define appropriate handling qualities metrics, flight characteristics of the vehicles, tailored MTEs and flight maneuvers, alterations to the environment (to include more levels of turbulence and visibility), impact of component failure, and sudden escalation of severe weather effects should all be considered.

These aspects could be explored further using analytical methods, fixed based simulation, and motion-based simulation, such as NASA Ames' VMS. Fixed based simulators are sufficient for the development process, however, motion-based simulators should be utilized once environment, atmospheric, and vehicle models are sufficiently mature because of the criticality of movement-based cueing and pilot workload in the proposed environment.

Many exciting and critical investigations could be matured with the use of motion-based simulators. However, because of potential impact to mission and current level of technology readiness, it is recommended that the following areas be prioritized in the near future for motion-based study: effect of varying levels of turbulence generated in a wildfire environment, control type impact on pilot workload, and adapted MTEs.

It was concluded that the RVLTL toolchain is flexible enough to be used for wildfire research given appropriate vehicle and environment models. Considering this, it may also be possible to apply the toolchain to other public good

topics such as earthquake/tornado relief, rescue from flood conditions, and remote medevac operations. Additionally, other tools within the RFLT toolchain such as propulsion/power systems, acoustics, and crash safety should be explored in the context of these missions that have the potential for such significant impact.

CONCLUDING REMARKS

As the number of wildfire incidents grows, so too does the danger they pose to first responders. Helicopters are a critical component of wildfire response which offer unique and advantageous capabilities. Feedback from firefighting pilots and a high-fidelity model of the environment are necessary for developing simulations which enable safe, experimental opportunities. This work provided a preliminary study addressing these issues by creating a representative wildfire turbulence model and leveraging the RFLT toolchain. This was accomplished using a conventional UH-60 as well as an AAM quadrotor designed with control laws to study the actuator requirements for providing Level 1 handling qualities performance.

A TRC response type was employed for each vehicle as it has the potential to reduce pilot workload. Based on estimates for potential turbulence severities, positional maintenance capabilities in a wildfire environment were estimated to vary between 4-15 feet for the conceptual quadrotor and 9-43 feet for the UH-60. Additionally, this study showed that, with the provided assumptions, actuator exceedances for this scenario varied 130-320% for the UH-60 and 620-980% for the quadrotor. Thus, both vehicles, as currently configured in this study, were found to be infeasible for the wildfire scenario. Both require their control systems to be redesigned with consideration of actuator limits, but the higher end of the exceedance estimate for the quadrotor suggests that a vehicle resizing may be a more likely requirement.

The success of this development cycle depends on the fidelity of the models being used. With future modeling advancements and the standardization of wildfire MTEs, estimates such as the ones presented in this study can be refined for several possibilities including prediction of regions for different levels of handling qualities within turbulent wildfire environments. Simulator studies involving firefighting pilots can help to validate these predictions and, subsequently, be used for experimentation and training to research best practices and mitigate risk.

Author contact: Jeremy Aires, jeremy.r.aires@nasa.gov
Shannah Withrow-Maser, shannah.n.withrow@nasa.gov
Nicholas Peters, nicholas.j.peters@nasa.gov

ACKNOWLEDGEMENTS

This work was supported by NASA's Revolutionary Vertical Lift Technology Project. Gratitude is extended to Carlos Malpica, Stefan Schuet, and David Caudle for technical guidance; Chris Silva and Wayne Johnson for creation of the NDARC models; Lauren Wagner, Sarah Conley, and Sesi Kottapalli for editorial review; and VTOL Analysis for Emergency Response Applications (VAERA) team members for insightful discussion.

REFERENCES

1. Silva, C. and Solis, E., "Aircraft Design Implications for Urban Air Mobility Vehicles Performing Public Good Missions," Vertical Flight Society's 80th Annual Forum & Technology Display, May 2024.
2. "First Use of a Helicopter for Firefighting – 26th, 1946", *National Wildfire Coordinating Group*, 2024 <https://www.nwcg.gov/committee/6mfs/first-use-of-helicopters-firefighting#:~:text=Summer%201946%20%E2%80%93%20Alaska%20Fire%20Service,helicopters%20for%20comprehensive%20firefighting%20duties>
3. Conley, S., Peters, N., Aires, J., Wagner, L., Kallstrom, K., Withrow-Maser, S., Wright, S., Radotich, M., Chianello, C., Ortiz, G., Ewing, G., Anderson, A., Klokkevold, K., Kluch, E., "VTOL Analysis for Emergency Response Applications (VAERA) – Identifying Technology Gaps for Wildfire Relief Rotorcraft Missions," Vertical Flight Society Sixth Decennial Aeromechanics Specialists' Conference, Santa Clara, CA, February 2024.
4. Butler, C., O'Conner, M., and Lincoln, J., 2015, "Aviation-Related Wildland Firefighter Fatalities", *Centers for Disease Control and Prevention*, 2015, <https://www.cdc.gov/mmwr/preview/mmwrhtml/mm6429a4.htm>
5. Church, C., Snow, J., and Dessens J., "Intense Atmospheric Vortices Associated with a 100 MW Fire", *Bulletin of the American Meteorological Society*, Vol. 61, 1980, [https://doi.org/10.1175/1520-0477\(1980\)061<0682:IAVAVA>2.0.CO;2](https://doi.org/10.1175/1520-0477(1980)061<0682:IAVAVA>2.0.CO;2)
6. Forthofer, J., and Goodrick, S., "Review of Vortices in Wildland Fire", *Journal of Combustion*, 2011, <https://doi.org/10.1038/s41598-022-13226-w>
7. Forthofer, J., "Fire Whirl Research", *Forest Service U.S. Department of Agriculture*, <https://www.firelab.org/project/fire-whirl-research>
8. Palacios, A., and Bradley, D., "Wildfires and the Generation of Fire Whirls", *Combustion and Flame*, Vol. 239, 2022, <https://doi.org/10.1016/j.combustflame.2021.111664>
9. Gaonkar, G., "Review of nonstationary gust-responses of flight vehicles." AIAA 21st Structures, Structural Dynamics, and Materials Conference, 1980, <https://doi.org/10.2514/6.1980-703>
10. Hohenemser, K., and Gaonkar, G., "Concepts for a theoretical and experimental study of lifting rotor

- random loads and vibrations”, Phase 1. No. NASA-CR-114707. 1967.
11. Rowe, S., Howson, D., and Turner, G., "A turbulence criterion for safe helicopter operations to offshore installations." *The Aeronautical Journal*. 2006;110(1113):749-758.
<https://doi.org/10.1017/S0001924000001615>
 12. Hess, Ronald A. "Simplified technique for modeling piloted rotorcraft operations near ships." *AIAA Journal of Guidance, Control, and Dynamics*, Vol. 29, No. 6, Nov. 2006, <https://doi.org/10.2514/1.18711>
 13. Withrow-Maser, S., et al., "Evaluation of heave disturbance rejection and control response criteria on the handling qualities evaluation of urban air mobility (AAM) eVTOL quadrotors using the Vertical Motion Simulator." Aeromechanics for Advanced Vertical Flight Technical Meeting, Transformative Vertical Flight, Feb. 2022.
 14. Malpica, C., et al., "Handling Qualities of Multicopter RPM-Controlled Electric-Vertical Take-Off and Landing (eVTOL) Aircraft for Urban Air Mobility (AAM)." Vertical Flight Society's 79th Annual Forum & Technology Display, May 2023.
 15. Aires, J., et al., "Analysis of handling qualities and power consumption for Urban Air Mobility (AAM) eVTOL quadrotors with degraded heave disturbance rejection and control response." Vertical Flight Society's 78th Annual Forum & Technology Display, May 2022.
 16. Johnson, W., and Silva, C., "NASA concept vehicles and the engineering of advanced air mobility aircraft", *The Aeronautical Journal*, 2022.
<https://doi.org/10.1017/aer.2021.92>
 17. Johnson, W. "NDARC — NASA Design and Analysis of Rotorcraft. Validation and Demonstration", American Helicopter Society Specialists' Conference on Aeromechanics, Jan. 2010.
 18. Anon., "Handling Qualities Requirements for Military Rotorcraft", Aeronautical Design Standard-33 (ADS-33E-PRF), US Army Aviation and Missile Command, March 2000.
 19. Lawrence, B., Theodore, C.R., and Johnson, W., T. Berger, T., "A Handling Qualities Analysis Tool for Rotorcraft Conceptual Designs", *The Aeronautical Journal*, Vol. 122, 2018.
<https://doi.org/10.1017/aer.2018.43>
 20. Seto, D., Clements, C., and Heilman, W., "Turbulence spectra measured during fire front passage", *Agricultural and Forest Meteorology*, Vol. 169, 2013.
<https://doi.org/10.1016/j.agrformet.2012.09.015>
 21. Hess, R., "Rotorcraft handling qualities in turbulence." *AIAA Journal of Guidance, Control, and Dynamics*, Vol. 18, No. 1, Jan. 1995.
<https://doi.org/10.2514/3.56654>
 22. Anon., "Flying Qualities of Piloted Aircraft", MIL-STD-1797A. U.S. Department of Defense, 1995
 23. Denis, M., and Pierson, W., "On the motions of ships in confused seas." *The Society of Naval Architects and Marine Engineers*, 1953,
<https://apps.dtic.mil/sti/citations/tr/AD0045880>
 24. Beal, T., "Digital simulation of atmospheric turbulence for Dryden and von Karman models." *AIAA Journal of Guidance, Control, and Dynamics*, Vol. 16, No. 1, 2012. <https://doi.org/10.2514/3.11437>
 25. Kim, F. D., Celi, R., and Tischler, M. B., "High Order State Space Simulation Model of Helicopter Flight Mechanics," *Journal of the American Helicopter Society*, Vol. 38, No 2, October 1993.
<https://doi.org/10.4050/JAHS.38.16>
 26. Anon., "Aerospace - Flight Control Systems - Design, Installation and Test of Piloted Military Aircraft, General Specification for, SAE Aerospace Standard," *AS94900*, July 2007.
 27. Anon., "Department of Defense Detail Specification Handling Qualities for Military Rotorcraft," *MIL-DTL-32742(AR)*, 9 March 2023.
 28. Schuet, S., Malpica, C., Aires, J. "A Gaussian Process Enhancement to Linear Parameter Varying Models." AIAA AVIATION Modeling and Simulation Technologies Conference, 2021.
<https://arc.aiaa.org/doi/10.2514/6.2021-3006>.
 29. Franklin, J. and Stortz., M. "Moving base simulation evaluation of translational rate command systems for STOVL aircraft in hover", June 1996.

APPENDIX A

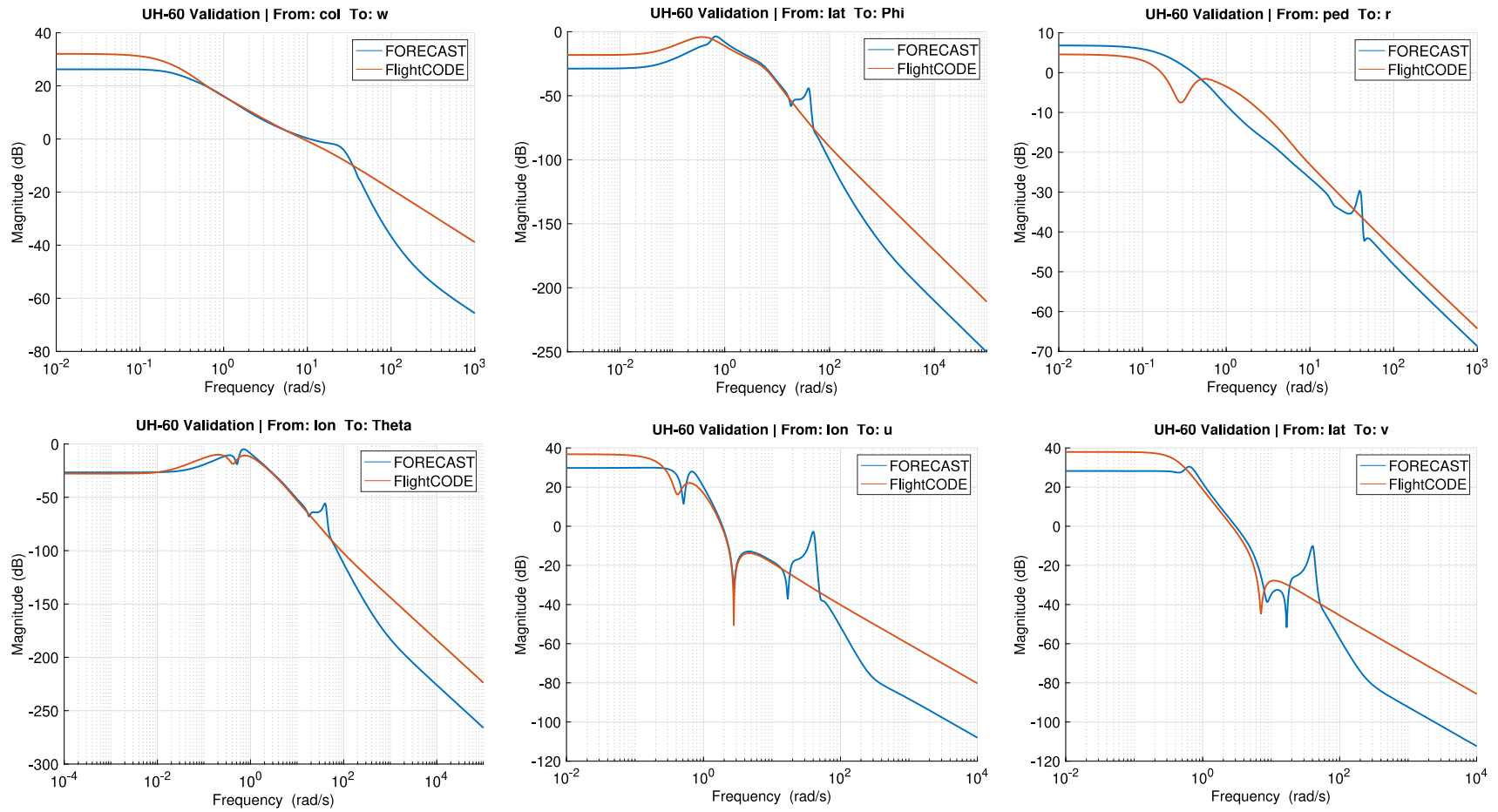


Fig. A1. FlightCODE UH-60 frequency response validation cases against FORECAST for all controlled axes.

APPENDIX B

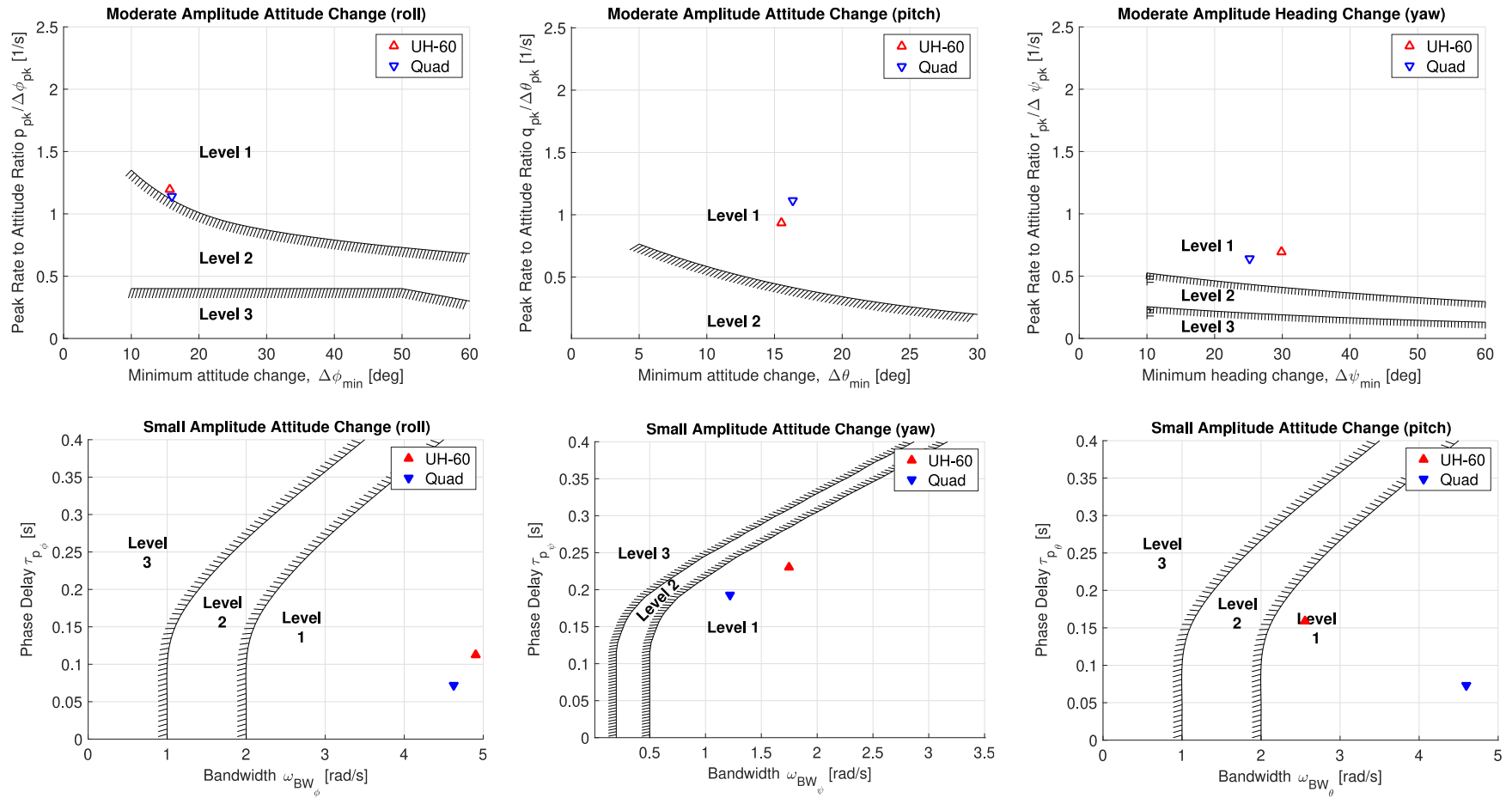


Fig. B1. Small and moderate-amplitude performance specification comparisons.

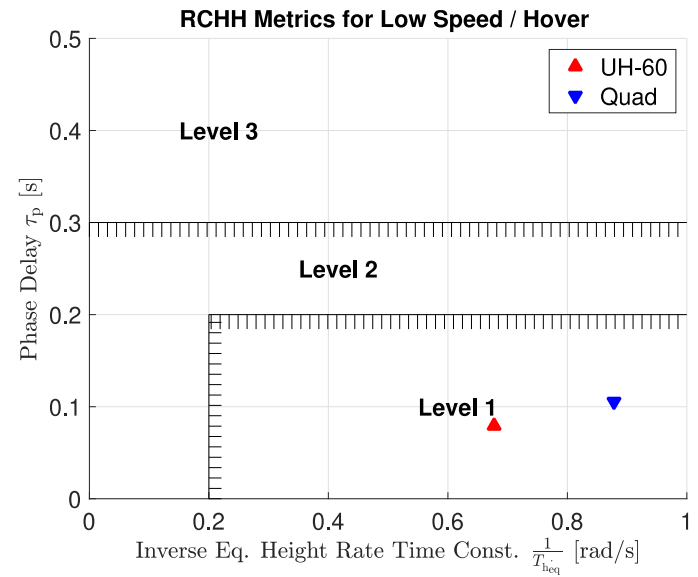
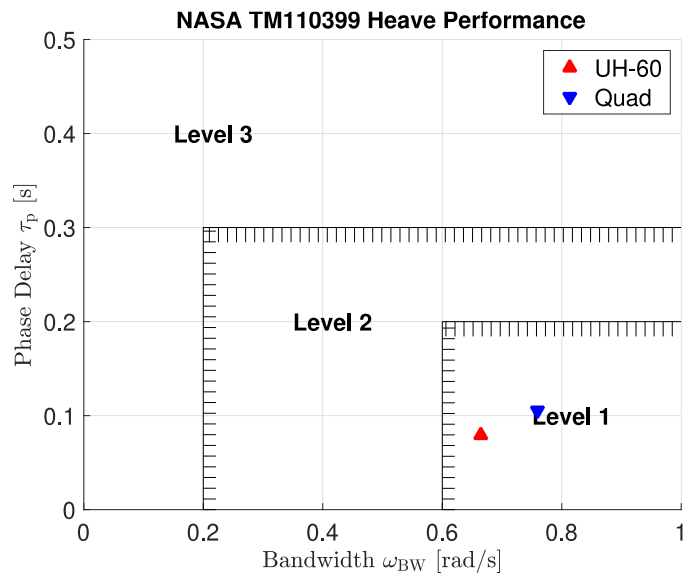
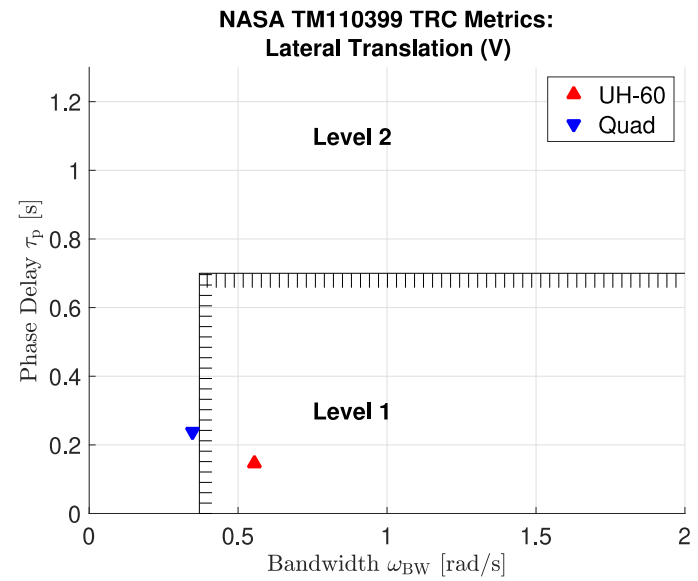
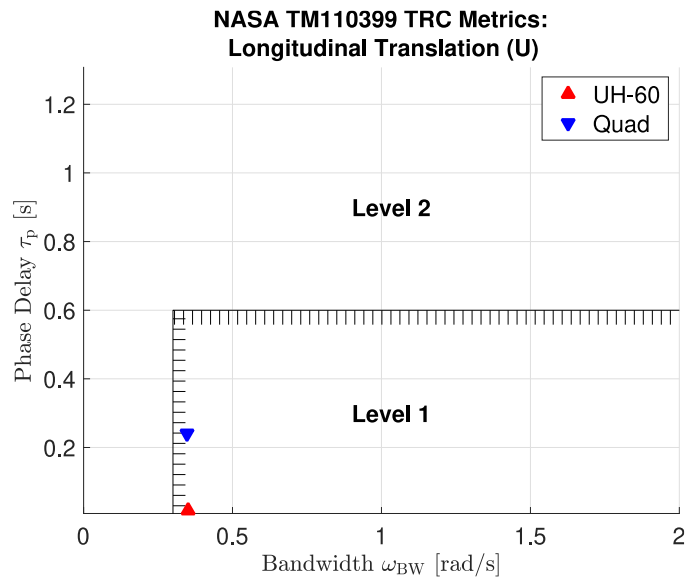


Fig. B2. Translational rate command and heave performance specification comparisons.

APPENDIX C

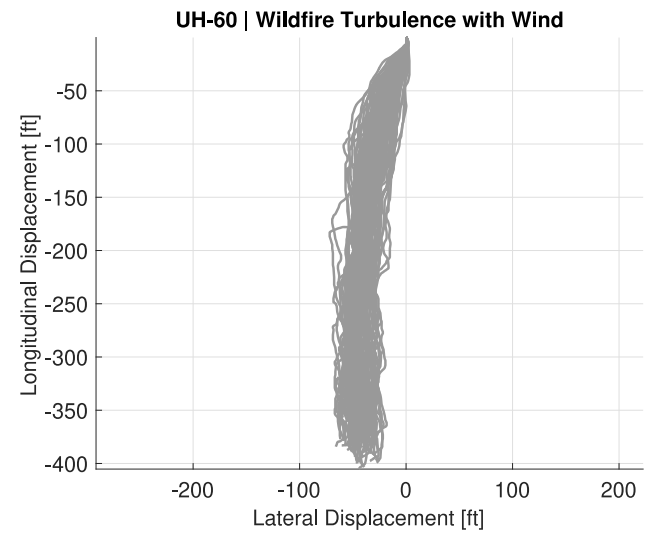
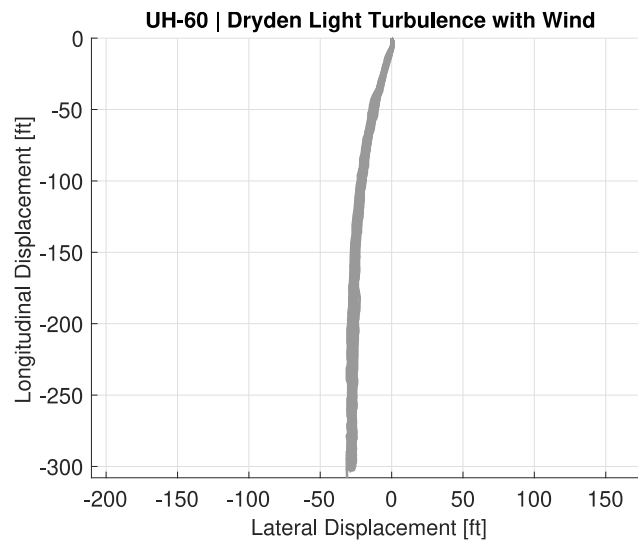
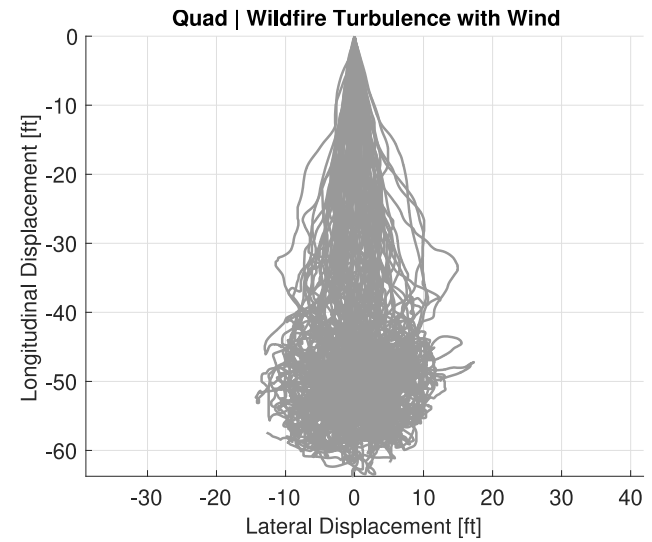
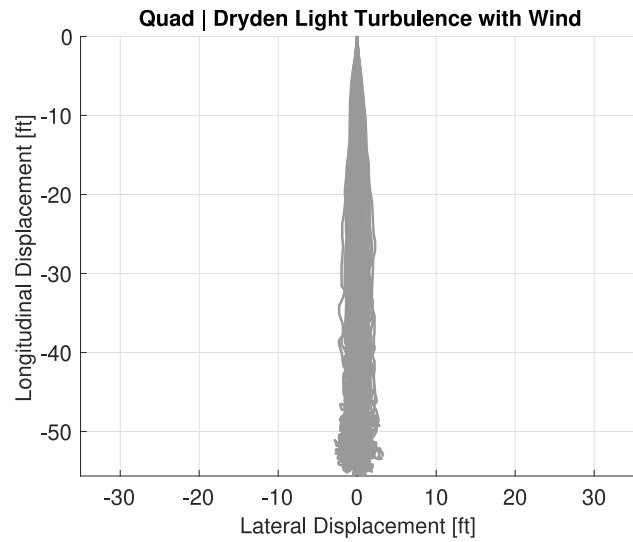


Fig. C1. XY-Positional deviation comparison charts for turbulence cases with wind.

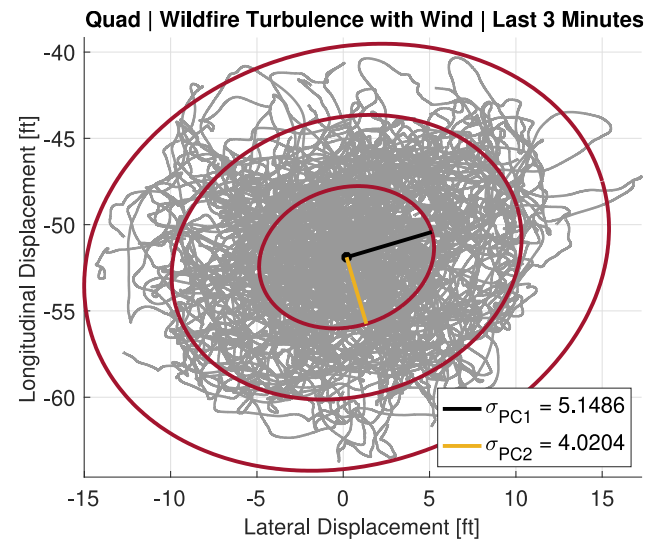
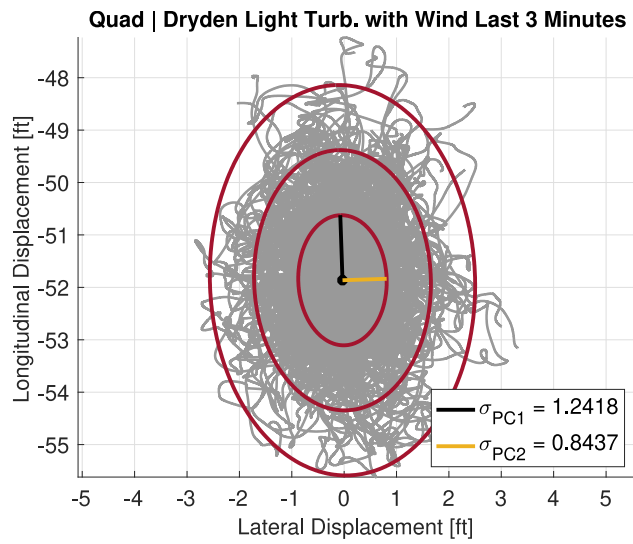


Fig. C2. Steady-state quadrotor XY-Positional deviation comparison charts for turbulence cases with wind.

APPENDIX D

Table D1. Deviation statistics for attitude (roll & pitch), heading (yaw), and altitude (height).

Roll Statistics [deg]					Pitch Statistics [deg]				
Vehicle / Turbulence	Mean	Std. Dev.	Max	Min	Vehicle / Turbulence	Mean	Std. Dev.	Max	Min
Quad / Wildfire + Wind	-2.52E-3	0.2118	0.7864	-0.8818	Quad / Wildfire + Wind	-1.1473	0.2436	0.0108	-2.1955
Quad / Wildfire	-2.50E-3	0.2184	0.8314	-0.9105	Quad / Wildfire	-7.51E-3	0.2190	0.8056	-1.0193
Quad / Dryden Light + Wind	-1.18E-4	0.0806	0.3186	-0.4036	Quad / Dryden Light + Wind	-1.1487	0.1442	0.0004	-1.8945
Quad / Dryden Light	-1.11E-4	0.0830	0.3235	-0.4123	Quad / Dryden Light	-8.02E-3	0.0993	0.4163	-0.5095
UH-60 / Wildfire + Wind	1.0203	0.5793	3.5302	-1.2722	UH-60 / Wildfire + Wind	-1.4753	0.5154	4.5572	-4.4098
UH-60 / Wildfire	0.0485	0.4694	3.8626	-3.1181	UH-60 / Wildfire	-0.0391	0.5051	3.1896	-4.0216
UH-60 / Dryden Light + Wind	1.0164	0.2633	2.0889	-0.7846	UH-60 / Dryden Light + Wind	-1.4707	0.3676	4.4020	-4.2989
UH-60 / Dryden Light	0.0147	0.1881	1.1249	-0.8458	UH-60 / Dryden Light	-8.58E-3	0.1881	1.0997	-1.7070

Yaw Statistics [deg]					Height Statistics [ft]				
Vehicle / Turbulence	Mean	Std. Dev.	Max	Min	Vehicle / Turbulence	Mean	Std. Dev.	Max	Min
Quad // Wildfire + Wind	1.05E-7	0.0005	0.0064	-0.0059	Quad / Wildfire + Wind	5.25E-4	0.0323	0.1738	-0.4740
Quad / Wildfire	5.12E-8	0.0004	0.0048	-0.0062	Quad / Wildfire	2.77E-5	0.0246	0.0990	-0.4750
Quad / Dryden Light + Wind	1.31E-7	0.0001	0.0010	-0.0009	Quad / Dryden Light + Wind	5.30E-4	0.0272	0.1395	-0.4727
Quad / Dryden Light	2.65E-8	0.0001	0.0010	-0.0011	Quad / Dryden Light	1.60E-5	0.0233	0.0814	-0.4746
UH-60 / Wildfire + Wind	-0.0104	0.3285	1.6809	-4.1455	UH-60 / Wildfire + Wind	0.0126	0.4825	4.1840	-1.8205
UH-60 / Wildfire	-2.62E-4	0.2539	1.6328	-2.4397	UH-60 / Wildfire	3.91E-4	0.2922	1.8167	-1.7031
UH-60 / Dryden Light + Wind	-0.0103	0.2599	1.3949	-3.9323	UH-60 / Dryden Light + Wind	0.0123	0.3286	3.9302	-1.0808
UH-60 / Dryden Light	-8.22E-5	0.0943	0.6304	-0.7302	UH-60 / Dryden Light	9.48E-5	0.1339	0.8887	-0.7432

Table D2. Deviation statistics for longitudinal (surge) and lateral (sway) translational rates.

Surge Statistics [ft/sec]					Sway Statistics [ft/sec]				
Vehicle / Turbulence	Mean	Std. Dev.	Max	Min	Vehicle / Turbulence	Mean	Std. Dev.	Max	Min
Quad / Wildfire + Wind	-0.1749	0.3789	0.8908	-2.1684	Quad / Wildfire + Wind	-1.74E-4	0.2278	0.8897	-0.8955
Quad / Wildfire	-1.70E-3	0.2286	0.9708	-0.9384	Quad / Wildfire	-2.18E-4	0.2349	0.9191	-0.9239
Quad / Dryden Light + Wind	-0.1745	0.3399	0.4360	-2.0469	Quad / Dryden Light + Wind	6.39E-4	0.1005	0.5290	-0.3939
Quad / Dryden Light	-1.30E-3	0.1162	0.5251	-0.4612	Quad / Dryden Light	6.60E-4	0.1036	0.5414	-0.4002
UH-60 / Wildfire + Wind	-1.2571	0.5158	0.8689	-3.1294	UH-60 / Wildfire + Wind	-0.1473	0.4705	1.6084	-2.3492
UH-60 / Wildfire	-0.0364	0.3351	1.5779	-2.4442	UH-60 / Wildfire	-5.10E-3	0.2603	1.1949	-1.0962
UH-60 / Dryden Light + Wind	-1.2492	0.3155	0.0000	-2.8726	UH-60 / Dryden Light + Wind	-0.1516	0.2761	0.8564	-1.3633
UH-60 / Dryden Light	-7.44E-3	0.1172	0.5565	-0.6604	UH-60 / Dryden Light	-2.18E-3	0.1167	0.4914	-0.5550